Electronic Supplementary Material (ESI) for CrystEngComm.

Electronic Supporting Information

Anion substitution in hydrogen-bonded organic conductors: Chemical pressure effect on hydrogen-bond-mediated phase transition

Junya Yoshida,*[a] Akira Ueda,*[a] Reiji Kumai,[b] Youichi Murakami,[b] and Hatsumi Mori*[a]

Email: jyoshida@issp.u-tokyo.ac.jp, a-ueda@issp.u-tokyo.ac.jp hmori@issp.u-tokyo.ac.jp,

[a]The Institute for Solid State Physics, The University of Tokyo, Kashiwa, Chiba 277-8581, Japan.

[b]CMRC and Photon Factory, Institute of Materials Structure Science, High Energy Accelerator Research Organization (KEK), Tsukuba, Ibaraki 305-0801, Japan.

Table S1 Comparison of crystallographic data for β'-[H_3(Cat-EDO-TTF)$_2$]BF_4 (**β'-BF_4**) at 270 K[S1] (high-temperature phase: HTP) and 240 K (HTP) and α-[H_3(Cat-EDO-TTF)$_2$]BF_4 (**α-BF_4**) at 150 K (low-temperature phase: LTP).[S1] See also Table 2 in the text.

	β'-BF_4[S1] (HTP)	**β'-BF_4** (HTP)	**α-BF_4**[S1] (LTP)
T / K	270	240	150
Formula	$C_{24}H_{15}O_8S_8B_1F_4$	$C_{24}H_{15}O_8S_8B_1F_4$	$C_{24}H_{15}O_8S_8B_1F_4$
Fw	774.66	774.66	774.66
Crystal System	Triclinic	Triclinic	triclinic
Space Group	*P*-1 (#2)	*P*-1 (#2)	*P*-1 (#2)
a / Å	7.2409(3)	7.2244(2)	7.1203(2)
b / Å	9.7683(5)	9.7489(3)	10.9390(4)
c / Å	10.8941(6)	10.8919(7)	18.0093(7)
α / °	66.6688(13)	66.737(1)	78.1857(8)
β / °	85.6578(18)	85.514(2)	82.3285(10)
γ / °	79.0863(19)	79.059(2)	89.7204(11)
V / Å^3	695.62(6)	691.94(6)	1358.06(8)
Z	1	1	2
d_{calc} / g·cm^{-3}	1.849	1.859	1.894
λ / Å	1.0000	1.0000	1.0000
$2\theta_{max}$ / °	91.4	74.2	74.1
R_{int}	0.0144	0.0153	0.0207
# of observations	2452	1726	3304
# of variables	232	236	473
R_1 [$I > 2.0\sigma(I)$]	0.0435	0.0381	0.0330
wR_2 (all data)	0.1348	0.1115	0.0958
GOF	1.060	1.097	1.048
CCDC	997839	1494927	997837

Table S2 Comparison of crystallographic data for β'-$[H_3(Cat\text{-}EDO\text{-}TTF)_2]ClO_4$ (**β'-ClO_4**) at 298 K and 150 K. See also Table 2 in the text.

	β'-ClO_4	**β'-ClO_4**
T / K	298	150
Formula	$C_{24}H_{15}ClO_{12}S_8$	$C_{24}H_{15}ClO_{12}S_8$
Fw	787.31	787.31
Crystal System	triclinic	triclinic
Space Group	*P*-1 (#2)	*P*-1 (#2)
a / Å	7.2808(4)	7.1809(5)
b / Å	9.8586(8)	9.8084(9)
c / Å	10.8660(8)	10.851(1)
α / °	66.382(2)	66.647(3)
β / °	85.050(3)	84.880(3)
γ / °	78.872(3)	78.699(3)
V / Å^3	701.15(9)	688.0(1)
Z	1	1
d_{calc} / g·cm^{-3}	1.864	1.900
λ / Å	1.0000	1.0000
$2\theta_{max}$ / º	83.6	74.2
R_{int}	0.0268	0.0305
# of observations	2159	1700
# of variables	236	236
R_1 [$I > 2.0\sigma(I)$]	0.0455	0.0446
wR_2 (all data)	0.1375	0.1323
GOF	1.097	1.104
CCDC	1494926	1494925

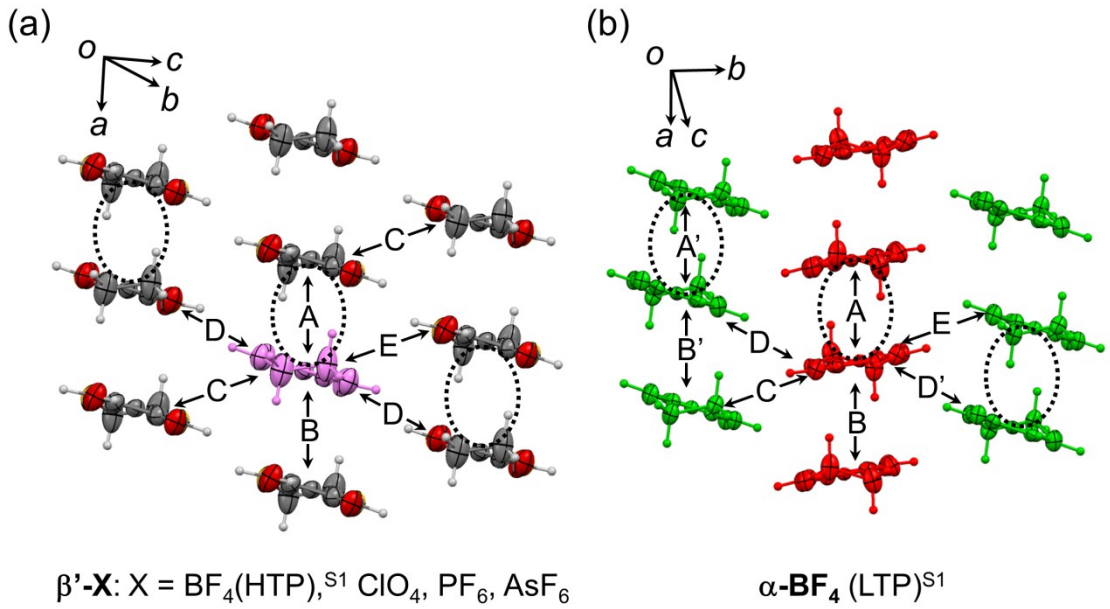

Fig. S1 Molecular arrangement in the conducting layer of (a) β'-[H_3(Cat-EDO-TTF)$_2$]X (**β'-X**: X = BF_4 (HTP),[S1] ClO_4, PF_6, AsF_6) and (b) **α-BF_4** (LTP).[S1] Value of the intermolecular transfer integrals (A (A'), B (B'), C, D (D'), and E) are shown in Table S3. Dotted circles represent the π-dimeric pairs.

Table S3 Comparison of intermolecular transfer integrals (see Fig. S1) of **β'-BF_4** at 270 K (HTP)[S1] and 240 K (HTP), **α-BF_4** at 150 K (LTP),[S1] and **β'-ClO_4** at 298 K and 150 K, calculated by using the extended Hückel method.[S2]

Transfer integral	**β'-BF_4**[S1] (270 K)	**β'-BF_4** (240 K)	**α-BF_4**[S1] (150 K)	**β'-ClO_4** (298 K)	**β'-ClO_4** (150 K)
A / meV	134	139	177 (A) 166 (A')	127	144
B / meV	4.3	6.8	4.0 (B) 43.8 (B')	3.0	3.8
C / meV	51.0	52.4	25.3	41.0	51.0
D / meV	0.7	0.5	0.13 (D) 6.5 (D')	0.7	0.6
E / meV	0.05	0.08	0.08	0.06	0.11

Table S4 Theoretical exchange coupling parameters ($2J \cdot k_B^{-1}$) within the π-dimers (dotted circles in Fig. S1) of **β'-X** (X = BF_4,[S1] ClO_4, PF_6, AsF_6) and **α-BF_4**, calculated with the equation, $J \cdot k_B^{-1} = (E_{BS} - E_T)/(\langle S^2 \rangle_T - \langle S^2 \rangle_{BS})$.[S3] The spin expectation values and total energies for the broken-symmetry (BS) singlet ($\langle S^2 \rangle_{BS}$ and E_{BS}) and triplet states ($\langle S^2 \rangle_T$ and E_T) were calculated at the UB3LYP/6-31G(d) level of theory[S4] using the molecular geometries taken from the X-ray data.

Compound	**β'-BF_4**[S1] (270 K)	**β'-ClO_4** (298 K)	**β'-PF_6** (270 K)	**β'-AsF_6** (270 K)
$\langle S^2 \rangle_{BS}$	0.7647	0.7784	0.7329	0.7512
$\langle S^2 \rangle_T$	2.0317	2.0307	2.0301	2.0309
E_{BS} / hartree	–4709.7664	–4709.7979	–4709.8913	–4709.8871
E_T / hartree	–4709.7627	–4709.7944	–4709.8872	–4709.8832
$E_{BS} - E_T$ / K	–1170.6	–1105.2	–1294.7	–1231.5
$2J \cdot k_B^{-1}$ / K	–1847.9	–1765.1	–1996.1	–1924.7

Compound	**α-BF_4**[S1] (red dimer, 150 K)	**α-BF_4**[S1] (green dimer, 150 K)
$\langle S^2 \rangle_{BS}$	0.72965	0.72956
$\langle S^2 \rangle_T$	2.0340	2.0339
E_{BS} / hartree	–4709.7703	–4709.7470
E_T / hartree	–4709.7658	–4709.7427
$E_{BS} - E_T$ / K	–1395.4	–1366.5
$2J \cdot k_B^{-1}$ / K	–2139.5	–2095.3

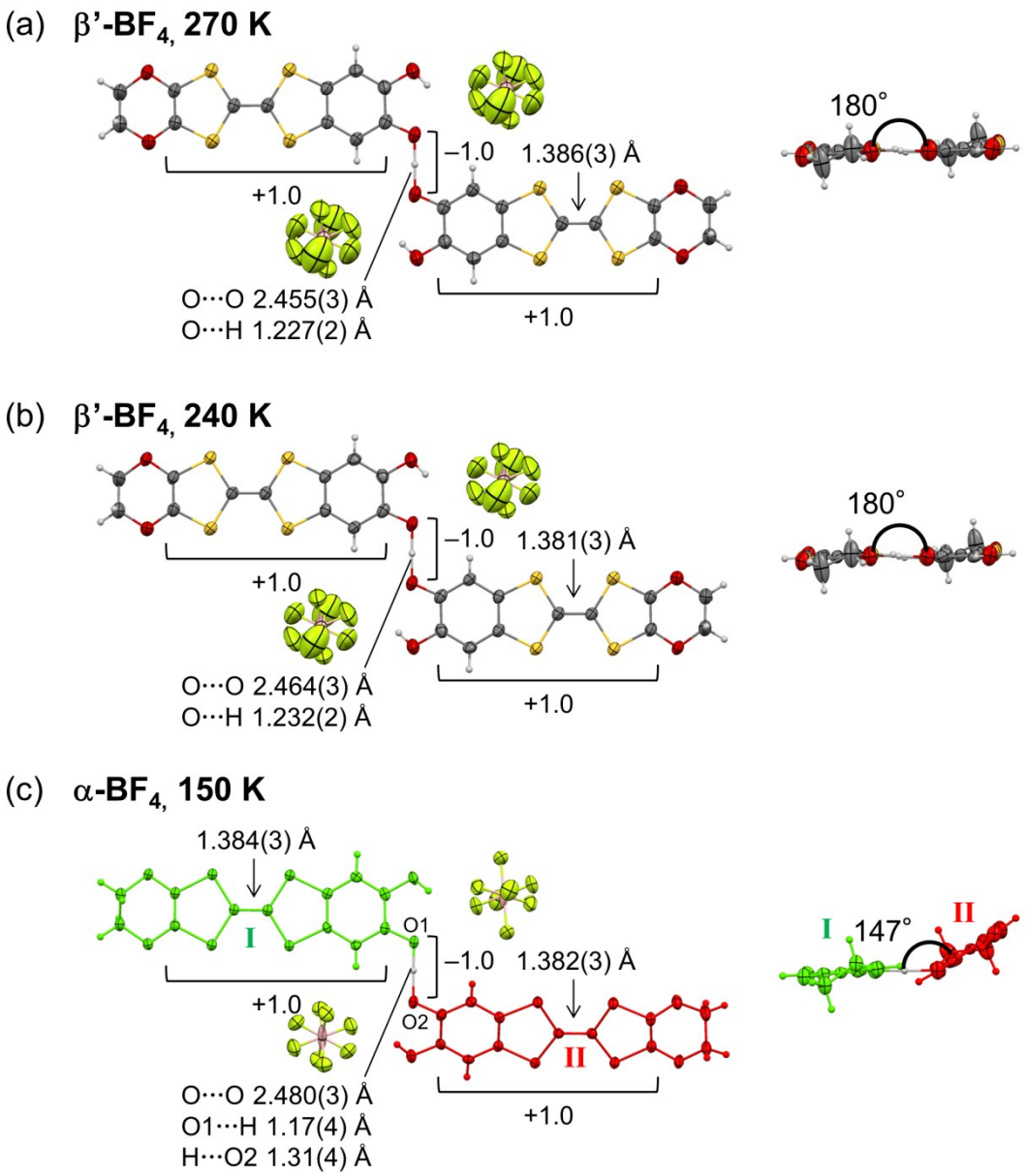

Fig. S2 X-ray crystal structures of the hydrogen-bonded (H-bonded) molecular unit in (a) **β'-BF_4** (270 K, HTP),[S1] (b) **β'-BF_4** (240 K, HTP), and (c) **α-BF_4** (150 K, LTP)[S1] (left: top view including the counter anions, right: side view).

The BF_4 anion is positionally and/or thermally disordered in both the HTP and LTP, which means that the anion dynamics is unchanged before and after the phase transition, and thus, this disordering should not participate in the phase transition. We also note that the temperature factors are decreased upon cooling, however, a similar decrease is also observed in **β'-ClO_4** without a phase transition (Fig. S3). Therefore, this temperature-factor change is not related to the occurrence of the phase transition.

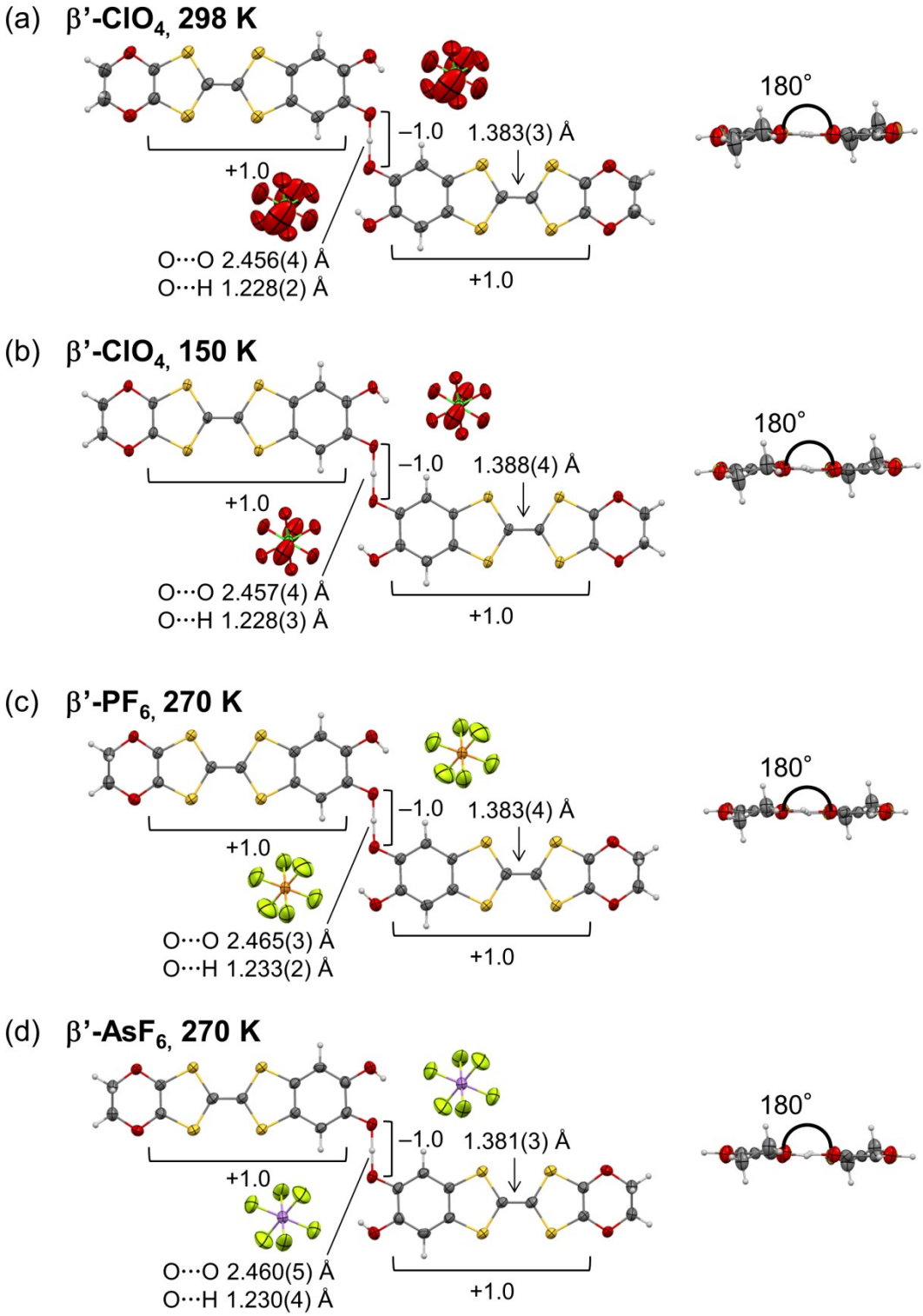

Fig. S3 Comparison of X-ray crystal structures of the H-bonded molecular unit in (a) **β'-ClO_4** (270 K), (b) **β'-ClO_4** (150 K), (c) **β'-PF_6** (270 K), and (d) **β'-AsF_6** (270 K) (left: top view including the counter anions, right: side view). See also Table 2 in the text.

The comparison among (a), (c), and (d) reveals that the H-bond distances (O···O = 2.456(4) ~ 2.465(3) Å) and the electrical charges on the TTF skeletons (+1, see also Table S4) are not influenced by the anion substitution. Also, the comparison between (a) and (b) shows that **β'-ClO_4** also undergoes a decrease in the temperature factors of the disordered counter anion, similar to the case of the BF_4 salt (Fig. S2).

Table S5 Charge estimation of the TTF skeleton in **β'-BF_4** (270 K,[S1] 240 K: HTP), **α-BF_4** (150 K: LTP),[S1] **β'-ClO_4** (298 K, 150 K), **β'-PF_6** (270 K), and **β'-AsF_6** (270 K), based on its bond lengths (*a*, *b*1, *b*2, *b*'1, *b*'2, *c*1, *c*2, *c*'1, *c*'2, *d*, and *d*'). The bond numbering scheme is given in Fig. S4. Values of δ and δ' are defined as (*b*1+*b*2)/2+(*c*1+*c*2)/2–*a*–*d* and (*b*'1+*b*'2)/2+(*c*'1+*c*'2)/2–*a*–*d*', respectively. Values of *Q*, *Q*', and *Q*" represent the tentative, net, and normalized electrical charges on the TTF skeleton, respectively, calculated with the equations[S1] shown below the Table.

The net charge *Q*' for the new compounds is calculated as 0.96(5) (at 298 K) and 0.96(5) (at 150 K) for **β'-ClO_4**, 0.95(5) (at 270 K) for **β'-PF_6**, and 0.92(6) (at 270 K) for **β'-AsF_6**. These values are suggestive of the +1 oxidized state, being consistent with the charge expected from the structural composition (Fig. S2 and S3). The details of the calculation are shown below the Table.

	β'-ClO_4 (298 K)	**β'-ClO_4** (150 K)	**β'-PF_6** (270 K)	**β'-AsF_6** (270 K)	Neutral Donor[S1] (298 K)
a / Å	1.383(3)	1.388(4)	1.383(4)	1.387(5)	1.347(8)
*b*1 / Å	1.729(2)	1.729(3	1.727(2)	1.724(4)	1.755(3)
*b*2 / Å	1.715(3)	1.720(4)	1.721(3)	1.720(5)	1.755(3)
b'1 / Å	1.717(3)	1.714(5)	1.724(2)	1.719(4)	1.770(3)
b'2 / Å	1.711(2)	1.730(3)	1.722(3)	1.720(5)	1.770(3)
*c*1 / Å	1.740(3)	1.737(3)	1.744(3)	1.738(4)	1.760(4)
*c*2 / Å	1.730(2)	1.741(4)	1.729(2)	1.733(3)	1.760(4)
c'1 / Å	1.722(3)	1.737(4)	1.730(3)	1.727(3)	1.756(4)
c'2 / Å	1.724(3)	1.733(3)	1.719(2)	1.729(4)	1.756(4)
d / Å	1.407(4)	1.410(6)	1.408(4)	1.399(7)	1.394(6)
d' / Å	1.340(5)	1.338(6)	1.350(4)	1.341(7)	1.315(6)
δ / Å	0.701(6)	0.666(8)	0.699(8)	0.70(1)	0.774(6)
δ' / Å	0.681(6)	0.731(8)	0.686(6)	0.69(1)	0.864(6)
Q [a]	1.19(3)	1.14(4)	1.18(3)	1.16(5)	0.24(3)
Q'[b]	0.96(5)	0.90(5)	0.95(5)	0.92(6)	0

	β'-BF_4[S1] (270 K: HTP)	**β'-BF_4** (240 K: HTP)	**α-BF_4**[S1] molecule I [d] (150 K: LTP)	**α-BF_4**[S1] molecule II [d] (150 K: LTP)
a / Å	1.386(3)	1.381(3)	1.384(3)	1.382(3)
*b*1 / Å	1.728(2)	1.718(4)	1.724(3)	1.728(3)
*b*2 / Å	1.714(3)	1.730(3)	1.726(3)	1.725(3)
b'1 / Å	1.722(3)	1.724(3)	1.723(3)	1.729(3)
b'2 / Å	1.723(2)	1.722(4)	1.729(3)	1.724(2)
*c*1 / Å	1.740(3)	1.741(3)	1.734(3)	1.734(3)
*c*2 / Å	1.729(2)	1.733(3)	1.744(2)	1.736(3)
c'1 / Å	1.722(3)	1.733(3)	1.724(3)	1.728(2)
c'2 / Å	1.731(3)	1.723(3)	1.731(2)	1.737(3)
d / Å	1.404(4)	1.402(5)	1.411(4)	1.403(5)
d' / Å	1.338(5)	1.341(5)	1.343(5)	1.336(5)
δ / Å	0.666(6)	0.678(7)	0.669(6)	0.677(7)
δ' / Å	0.725(7)	0.729(7)	0.727(7)	0.741(6)
Q [a]	1.16(3)	1.10(4)	1.14(3)	1.06(3)
Q'[b]	0.92(5)	0.86(5)	0.90(5)	0.82(5)
Q'' [c]	–	–	1.05(7)	0.95(7)

[a] $Q = 6.347–7.463\cdot(\delta+\delta')/2$, [b] $Q' = Q–0.235$. [c] Q''(molecule I) = [Q'(molecule I)/(Q'(molecule I) + Q'(molecule II))] × 2, Q''(molecule II) = [Q'(molecule II)/(Q'(molecule I) + Q'(molecule II))] × 2. [d] molecule I, II are shown in Fig. S2c.

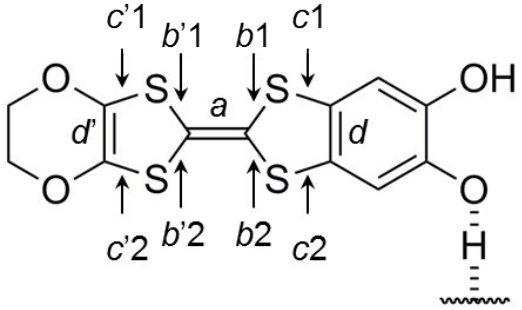

Fig. S4 Bond numbering scheme for the TTF skeleton.

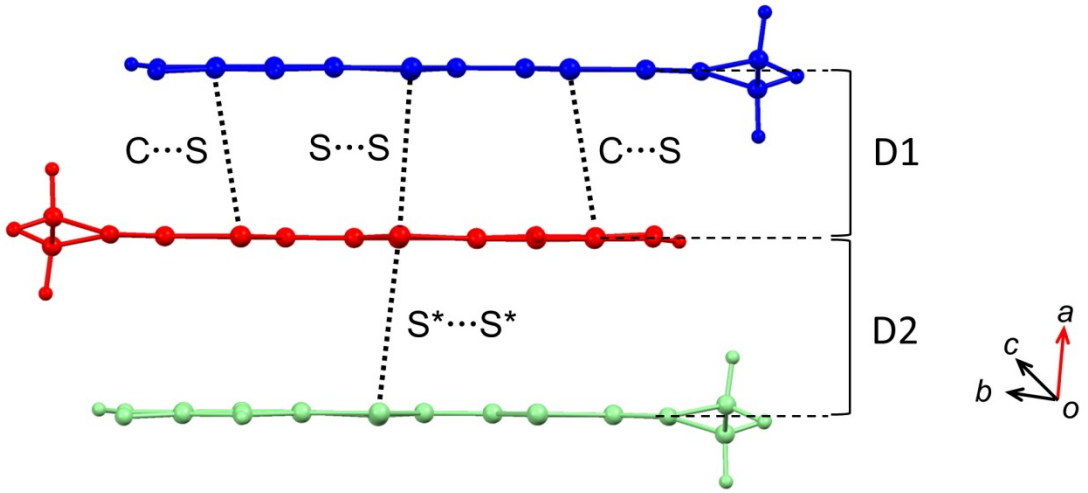

Fig. S5 π-Stacking column along the *a* axis in **β'-X** (**X** = BF_4,[S1] ClO_4, PF_6, AsF_6). Dotted lines represent the intermolecular contacts (S···S, C···S, S*···S*). D1 and D2 represent the interplaner distances of the TTF skeletons, corresponding to the interactions A and B in Fig. S1a, respectively. These parameters are not significantly changed by the anion substitution, as shown in Table S6.

Table S6 Comparison of the intermolecular contacts (S···S, C···S, S*···S* in Fig. S5) and interplanar distances (D1, D2 in Fig. S5) in **β'-X** (**X** = BF_4,[S1] ClO_4, PF_6, AsF_6).

X	BF_4 (270 K)[S1]	ClO_4 (298 K)	PF_6 (270 K)	AsF_6 (270 K)
S···S / Å	3.451(1)	3.472(1)	3.461(1)	3.456(2)
C···S / Å	3.473(4)	3.472(4)	3.423(4)	3.407(5)
S*···S* / Å	3.813(1)	3.861(1)	3.813(1)	3.792(2)
D1 / Å	3.39~3.40	3.39~3.41	3.37~3.41	3.36~3.41
D2 / Å	3.61~3.62	3.59~3.61	3.53~3.57	3.52~3.57

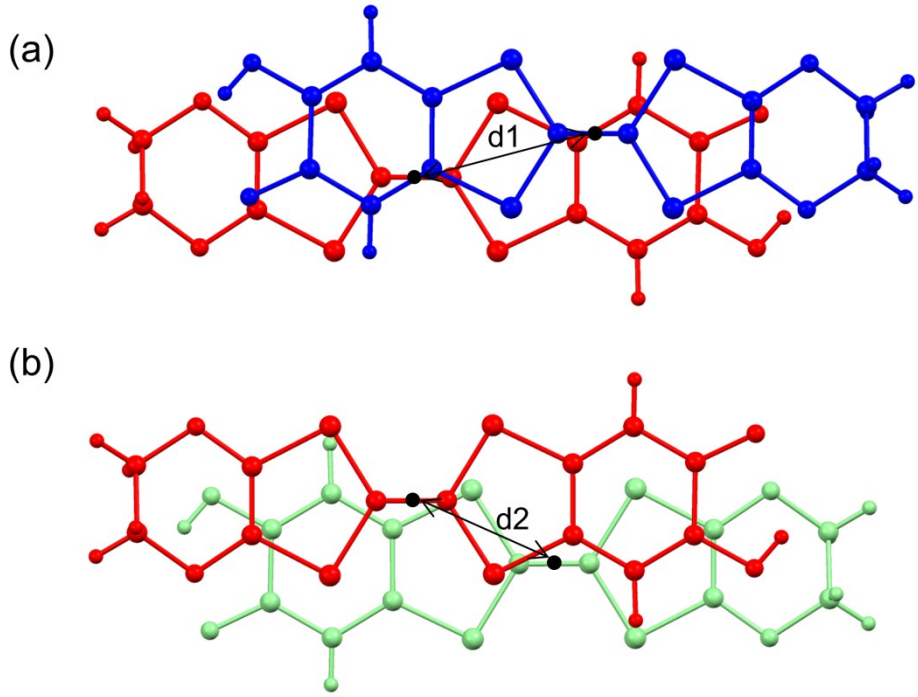

Fig. S6 Overlapping modes (a) within the π-dimer (the D1 direction in Fig. S5) and (b) between the π-dimers (the D2 direction in Fig. S5) in **β'-X** (**X** = BF_4,[S1] ClO_4, PF_6, AsF_6). Distances of d1 and d2 measured between the centers of the central C=C bond in the TTF skeleton represent the intermolecular distances. These distances are not significantly changed by the anion substitution, as shown in Table S7.

Table S7 Comparison of intermolecular distances (d1, d2 in Fig. S6) in **β'-X** (**X** = BF_4,[S1] ClO_4, PF_6, AsF_6).

	BF_4 (270 K)[S1]	ClO_4 (298 K)	PF_6 (270 K)	AsF_6 (270 K)
d1 / Å	3.41	3.42	3.41	3.40
d2 / Å	3.60	3.58	3.54	3.53

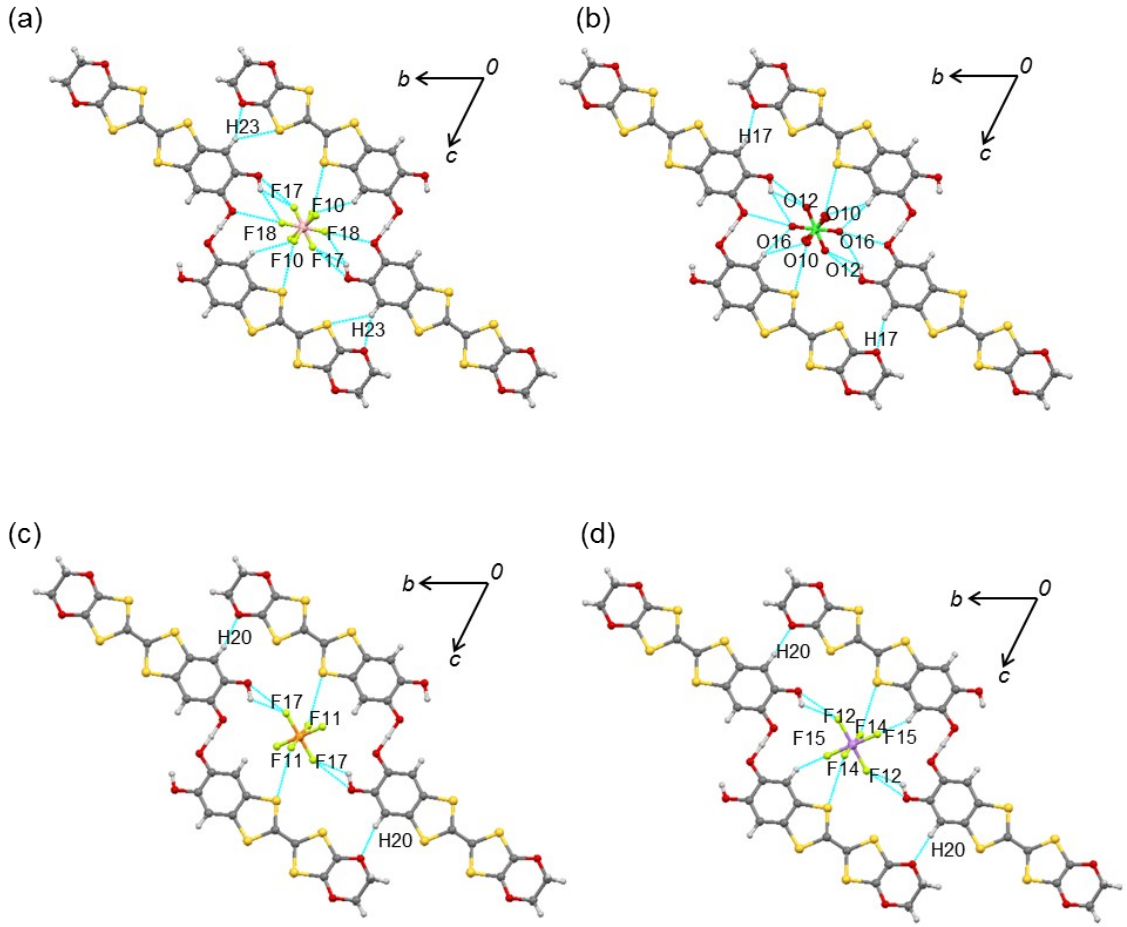

Fig. S7 Crystal packing structures around the counter anion in **β'-X** (**X** = (a) $\mathbf{BF_4}$ (270 K),[S1] (b) $\mathbf{ClO_4}$ (298 K), (c) $\mathbf{PF_6}$ (270 K), (d) $\mathbf{AsF_6}$ (270 K)) in the *bc* plane. Blue lines represent the interatomic contacts shorter than the sum of van der Waals (vdW) radii.

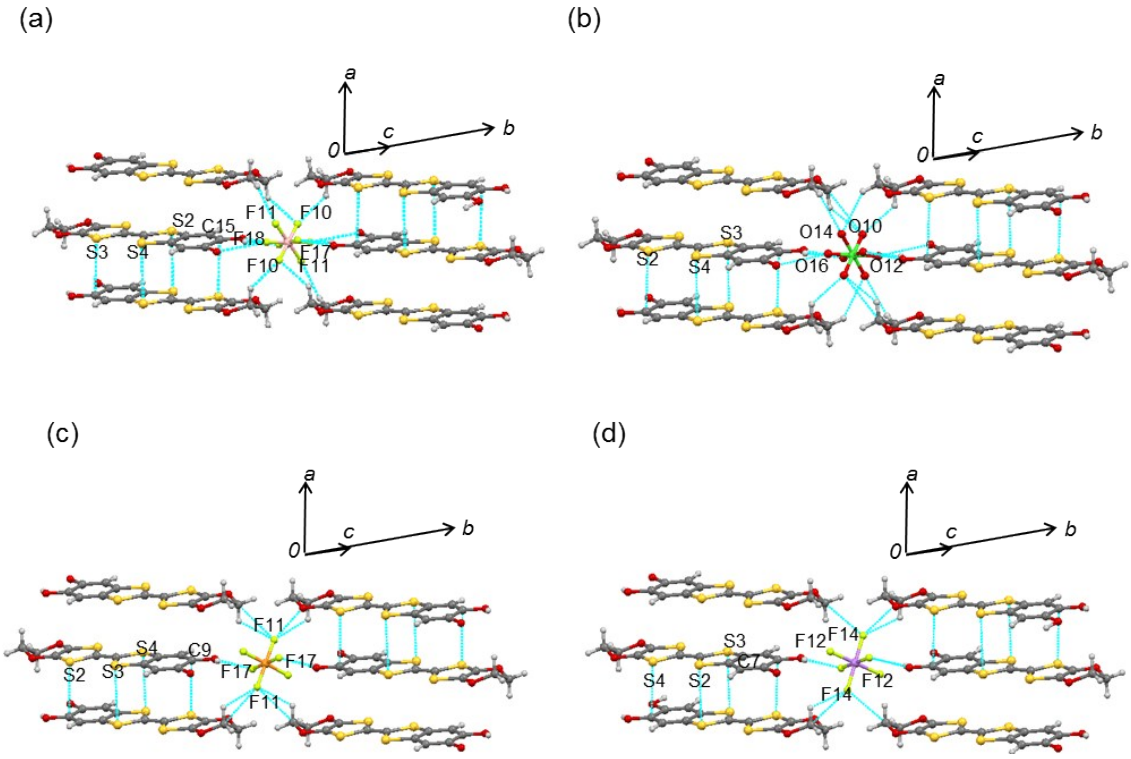

Fig. S8 Crystal packing structures around the counter anion in **β'-X** (**X** = (a) $\mathbf{BF_4}$ (270 K),[S1] (b) $\mathbf{ClO_4}$ (298 K), (c) $\mathbf{PF_6}$ (270 K), (d) $\mathbf{AsF_6}$ (270 K)). Blue lines represent the interatomic contacts shorter than the sum of vdW radii.

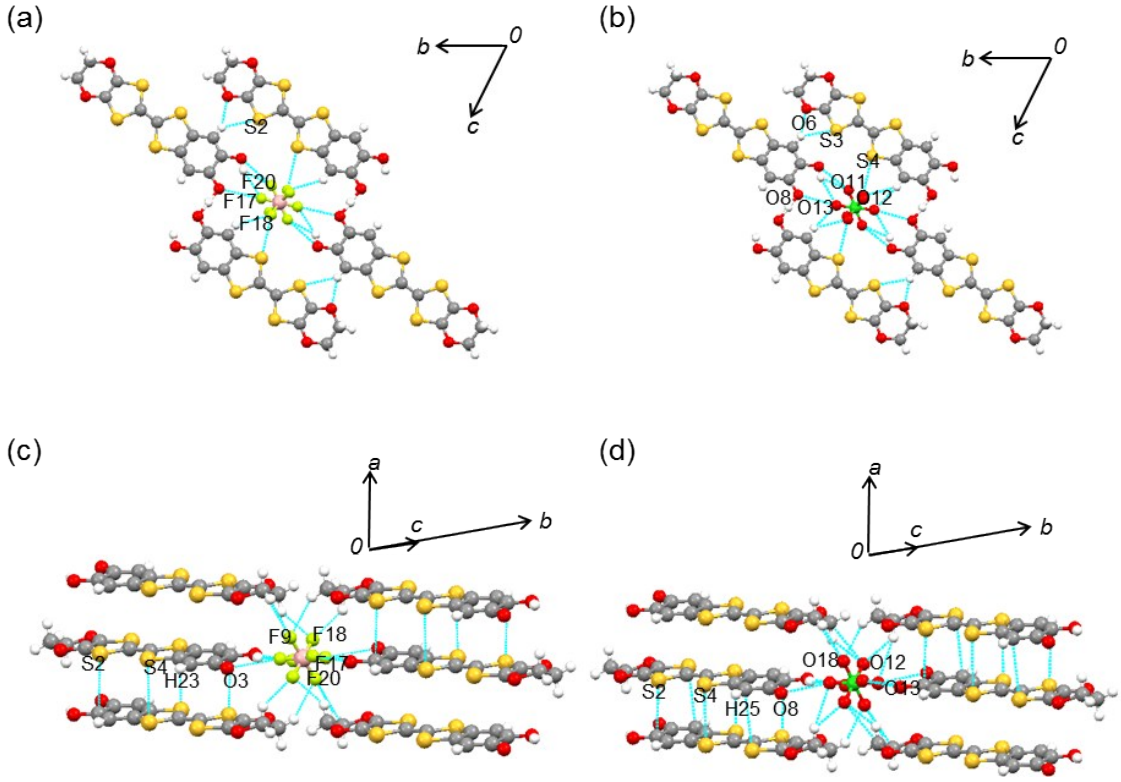

Fig. S9 Crystal packing structures around the counter anion in the *bc* plane of (a) **β'-BF_4** (240 K) and (b) **β'-ClO_4** (150 K), and along the *a*-axis of (c) **β'-BF_4** (240 K) and (d) **β'-ClO_4** (150 K). Blue lines represent the interatomic contacts shorter than the sum of vdW radii.

The interatomic contacts including H-bonding interactions contract anisotropically with decreasing temperature. The contacts along the *b*-axis contract, whereas that along the *c*-axis has no change. As for **β'-BF_4** [**β'-ClO_4**], the contacts (F17---O25) and (F18---O25) [(F17---O25) and (F18---O25)] change from 2.764(7) Å and 2.982(7) Å [2.766(7) Å and 2.961(8) Å] at 270 K [298 K] (Fig. S7 and S8, Table S8) to 2.757(7) Å and 2.966(7) Å [2.758(6) Å and 2.903(8) Å] at 240 K [150 K], while the contact (F10---S4) [(O10---S4)] has no change from 3.126(6) Å [3.126(8) Å] at 270 K [298 K] to 3.126(6) Å [3.126(8) Å] at 240 K [150 K], which is good agreement with the anisotropic chemical pressure along the *b*-axis.

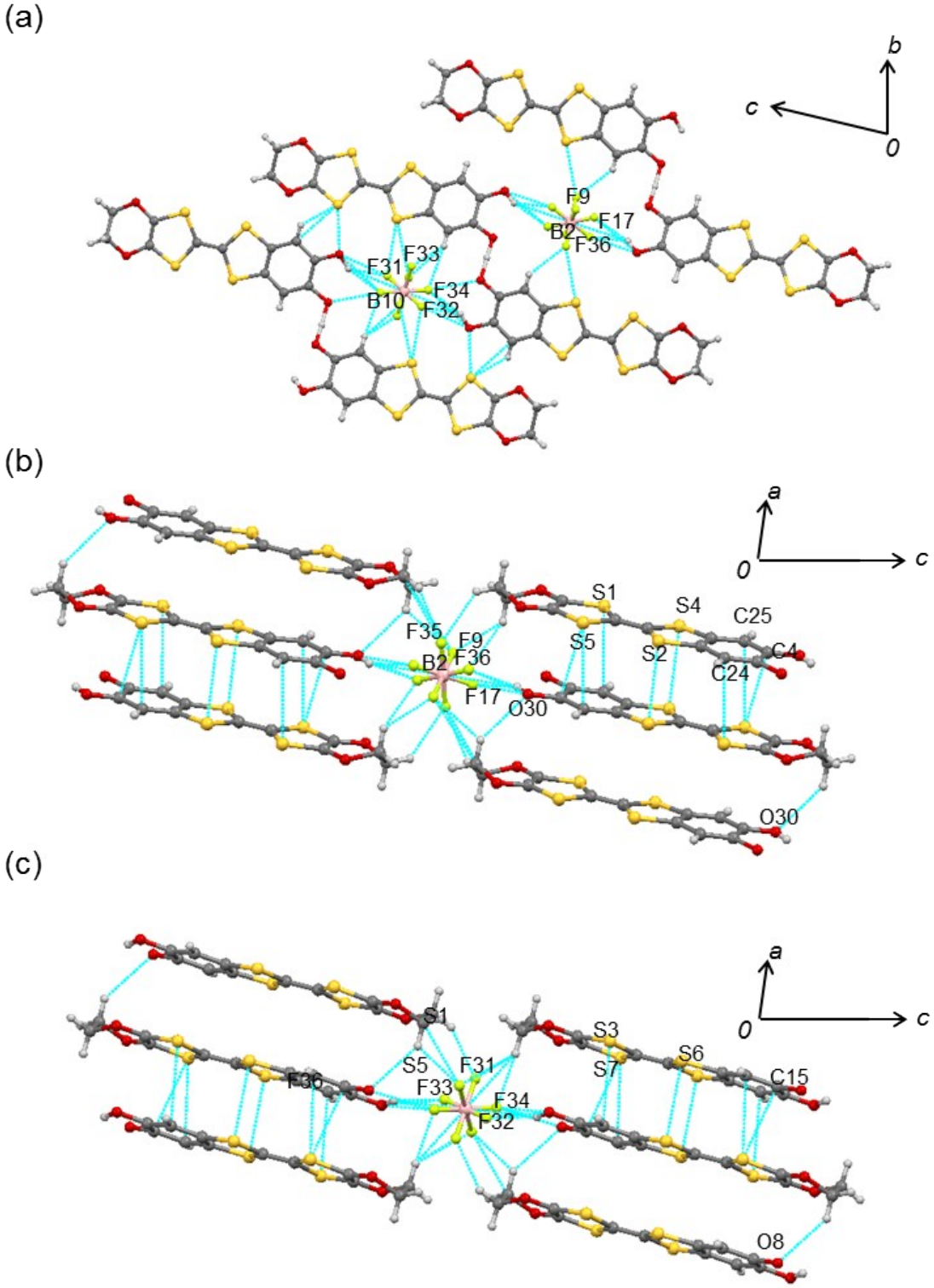

Fig. S10 Crystal packing structures around the BF_4 anion in **α-BF_4** (150 K),[S1] (a) in the *bc* plane and (b), (c) along the *b*-axis. Blue lines represent the interatomic contacts shorter than the sum of vdW radii.

Table S8 Comparison of intermolecular distances (Fig. S7-S10) in **β'-X** (**X** = BF_4,[S1] ClO_4, PF_6, AsF_6) and **α-BF_4**.

β'-$[H_3(Cat\text{-}EDO\text{-}TTF)_2]BF_4$ (270 K)[S1]			
	d [(F / O)…H] / Å	*d* [H−(O / C)] / Å	∠[(F / O)…H−(O / C)] /°
F17···H22−O25	2.19(3)	0.82(3)	127(4)
F18···H22−O25	2.28(3)	0.82(3)	154(4)
F10···H21−C16	2.54(4)	0.90(4)	142(2)
F10···H7B−C7	2.528(6)	0.970(6)	136.4(2)
F10···H8A−C8	2.432(6)	0.970(6)	133.9(3)
F11···H7A−C7	2.41(1)	0.970(5)	138.8(5)
O14···H23−C15	2.64(4)	0.94(4)	150(3)
	d / Å		
F10···S4	3.126(6)		
F17···O25	2.764(7)		
F18···O2	2.982(7)		
S3···H23	2.96(4)		
S3···C15	3.557(4)		
S2···S4	3.451(2)		

β'-$[H_3(Cat\text{-}EDO\text{-}TTF)_2]BF_4$ (240 K)			
	d [(F / O)…H] / Å	*d* [H−(O / C)] / Å	∠[(F / O)…H−(O or C)] /°
F20···H21−O4	2.17(3)	0.83(4)	128(4)
F17···H21−O4	2.25(3)	0.83(4)	155(4)
F18···H23−C15	2.53(4)	0.88(4)	143(2)
F18···H6B−C6	2.436(6)	0.970(7)	134.8(3)
F9···H10A−C10	2.368(9)	0.970(5)	138.2(5)
F9···H6A−C6	2.60(1)	0.970(6)	145.7(4)
F18···H10B−C10	2.532(6)	0.970(6)	136.2(2)
O13···H22−C16	2.70(4)	0.91(4)	144(2)
	d / Å		
F10···S4	3.107(6)		
F17···O3	2.966(7)		
F20···O4	2.757(6)		
S2···H22	2.98(4)		
S2···C7	3.467(4)		
F9···C10	3.16(1)		

S1···S4	3.441(1)

α-$[H_3(Cat\text{-}EDO\text{-}TTF)_2]BF_4$ (150 K) [S1]			
	d [(F / O)…H] / Å	*d* [H−(O / C)] / Å	∠[(F / O)…H−(O / C)] /°
F17···H40−O30	2.17(4)	0.82(4)	153(3)
F36···H40−O30	2.06(4)	0.82(4)	135(3)
F9···H38−C27	2.59(3)	0.84(4)	133(3)
F35···H5A−C5	2.633(6)	0.970(6)	125.1(4)
F35···H5B−C5	2.769(6)	0.970(6)	107.1(3)
F35···H1A−C1	3.210(6)	0.970(5)	109.2(4)
F33···H42−C24	2.59(3)	0.89(3)	137(3)
F31···H42−C24	2.53(2)	0.89(3)	136(2)
F34···H42−C24	2.50(3)	0.89(3)	173(3)
F32···H39−O5	2.10(4)	0.92(5)	133(3)
F9···H1B−C1	2.555(5)	0.970(5)	130.5(3)
F36···H1B−C1	2.582(6)	0.970(5)	140.6(3)
O30···H58−C5	2.657(4)	0.970(5)	145.2(3)
F31···H7A−C7	2.370(5)	0.970(4)	139.7(4)
F31···H7B−C7	2.660(5)	0.970(6)	123.0(4)
F33···H11B−C11	2.466(5)	0.970(6)	119.2(3)
F34···H7B−C7	2.538(7)	0.970(7)	154.8(4)
F11···H7A−C7	2.695(4)	0.970(7)	145.6(3)
O8···H11B−C11	2.695(4)	0.970(7)	145.6(3)
	d / Å		
F9···S6	3.162(4)		
F17···O30	2.917(5)		
F36···O30	2.693(4)		
F31···S2	3.124(4)		
F34···O8	2.827(4)		
F32···O5	2.811(5)		
F32···S2	3.198(5)		
S5···O5	3.252(3)		
S5···H37	2.96(3)		
S5···C26	3.359(3)		
F35···C5	3.192(6)		
F35···C1	3.112(6)		

S5···C4	3.468(3)
S5···C25	3.466(3)
S1···C24	3.472(3)
S2···S4	3.384(2)
F33···C11	3.059(6)
F3···C26	3.672(3)
S6···S8	3.788(2)
S7···C27	3.734(4)
S7···C15	3.374(3)

β'-$[H_3(Cat\text{-}EDO\text{-}TTF)_2]ClO_4$ (298 K)

	d [O…H] / Å	*d* [H−(O / C)] / Å	∠[O…H−(O / C)] / °
O12···H20−O3	2.26(4)	0.81(4)	120(4)
O16···H20−O3	2.37(4)	0.81(4)	152(5)
O10···H18−C15	2.60(5)	0.93(4)	139(3)
O10···H9B−C9	2.561(9)	0.970(7)	132.3(4)
O10···H3B−C3	2.486(8)	0.970(7)	128.5(4)
O14···H9A−C9	2.47(2)	0.970(5)	136.7(5)
O14···H3A−C3	2.69(2)	0.970(6)	141.7(6)
O1···H17−O13	2.61(5)	0.98(5)	146(3)

	d / Å
O10···S4	3.126(8)
O12···O3	2.766(7)
O16···O5	2.961(8)
O10···C3	3.182(9)
S3···S4	3.472(2)
S2···C6	3.472(4)

β'-$[H_3(Cat\text{-}EDO\text{-}TTF)_2]ClO_4$ (150 K)

	d [O…H] / Å	*d* [H−(O / C)] / Å	∠[O…H−(O / C)] / °
O11···H9−O9	2.20(4)	0.83(4)	125(5)
O13···H9−O9	2.29(4)	0.83(4)	159(6)
O13···H25−C25	2.63(6)	0.93(5)	167(4)
O10···H14B−C14	2.55(5)	0.970(6)	141(4)
O10···H20B−C20	2.37(4)	0.970(4)	134(4)
O12···H20A−C20	2.521(7)	0.970(6)	130(4)
O12···H14A−C14	2.42(4)	0.97(5)	128(4)

O13···H20A−O20	2.903(8)	0.97(5)	160(5)
O12···H25−C25	2.52(5)	0.93(5)	140(3)
O6···H22−O22	2.95(5)	1.00(5)	144(3)

	d / Å
O12···S4	3.165(7)
O11···O9	2.758(6)
O13···O8	2.903(8)
S2···S4	3.422(2)
S3···C17	3.433(5)
S3···H22	2.95(9)
O10···C20	3.12(1)
O12···C14	3.114(8)
S5···C25	3.481(5)

β'-[H_3(Cat-EDO-TTF)$_2$]PF_6 (270 K)

	d [(F / O)…H] / Å	*d* [H−(O / C)] / Å	∠[(F / O)…H−(O / C)] /°
F17···H22−O3	2.24(4)	0.93(4)	122(4)
F11···H13B−C13	2.632(4)	0.970(5)	112.5(3)
F11···H12B−C12	2.531(5)	0.970(6)	119.3(3)
O16···H20−C19	2.49(4)	0.94(5)	158(3)

	d / Å
F11···S3	3.162(4)
F17···O3	2.842(3)
F11···C12	3.122(5)
F11···C13	3.135(5)
S2···D9	3.423(3)
S3···S4	3.461(2)

β'-[H_3(Cat-EDO-TTF)$_2$]AsF_6 (270 K)

	d [(F / O)…H] / Å	*d* [H−(O / C)] / Å	∠[F…H−(O / C)] /°
F12···H22−O18	2.29(6)	0.79(5)	128(6)
F14···H13A−C13	2.563(4)	0.970(7)	115.2(3)
O16···H20−C19	2.49(4)	0.94(5)	158(3)

	d / Å
F14···S2	3.18(5)
F12···O18	2.850(4)

F14···C13	3.102(7)
F14···C11	3.113(6)
S4···C7	3.407(5)
S2···S3	3.456(2)

Reference

[S1] J. Yoshida, A. Ueda, A. Nakao, R. Kumai, H. Nakao, Y. Murakami, H. Mori, *Chem. Commun.* **2014**, *50*, 15557–15560.

[S2] T. Mori, A. Kobayashi, Y. Sasaki, H. Kobayashi, G. Saito, H. Inokuchi, *Bull. Chem. Soc. Jpn.* **1984**, *57*, 627–633.

[S3] S. Yamanaka, T. Kawakami, H. Nagao, K. Yamaguchi, *Chem. Phys. Lett.* **1994**, 231, 25–33.

[S4] M. J. Frisch, G. W. Trucks, H. B. Schlegel, G. E. Scuseria, M. A. Robb, J. R. Cheeseman, J. A. Montgomery, T. Vreven, K. N. Kudin, J. C. Burant, J. M. Millam, S. S. Iyengar, J. Tomasi, V. Barone, B. Mennucci, M. Cossi, G. Scalmani, N. Rega, G. A. Petersson, H. Nakatsuji, M. Hada, M. Ehara, K. Toyota, R. Fukuda, J. Hasegawa, M. Ishida, T. Nakajima, Y. Honda, O. Kitao, H. Nakai, M. Klene, X. Li, J. E. Knox, H. P. Hratchian, J. B. Cross, V. Bakken, C. Adamo, J. Jaramillo, R. Gomperts, R. E. Stratmann, O. Yazyev, A. J. Austin, R. Cammi, C. Pomelli, J. W. Ochterski, P. Y. Ayala, K. Morokuma, G. A. Voth, P. Salvador, J. J. Dannenberg, V. G. Zakrzewski, S. Dapprich, A. D. Daniels, M. C. Strain, O. Farkas, D. K. Malick, A. D. Rabuck, K. Raghavachari, J. B. Foresman, J. V. Ortiz, Q. Cui, A. G. Baboul, S. Clifford, J. Cioslowski, B. B. Stefanov, G. Liu, A. Liashenko, P. Piskorz, I. Komaromi, R. L. Martin, D. J. Fox, T. Keith, M. A. Al-Laham, C. Y. Peng, A. Nanayakkara, M. Challacombe, P. M. W. Gill, B. Johnson, W. Chen, M. W. Wong, C. Gonzalez, J. A. Pople, Gaussian, Inc., Wallingford CT, **2004**.